Green Chemistry

Improved Slit-shaped Microseparator and its Integration with a Microreactor for Modular Biomanufacturing

Journal:	*Green Chemistry*
Manuscript ID	GC-ART-02-2021-000642.R2
Article Type:	Paper
Date Submitted by the Author:	26-Apr-2021
Complete List of Authors:	Bhattacharyya, Souryadeep; University of Delaware, Department of Chemical and Biomolecular Engineering Desir, Pierre; Univ. of Delaware, Chemical and Biomolecular Engineering; Catalysis Center for Energy Innovation Prodinger, Sebastian; University of Delaware, Department of Chemical and Biomolecular Engineering Lobo, Raul; University of Delaware, Department of Chemical Engineering; University of Delaware Vlachos, Dion; Univ. of Delaware,

Improved Slit-shaped Microseparator and its Integration with a Microreactor for Modular Biomanufacturing

Souryadeep Bhattacharyya,[1,2] Pierre Desir, [1,2] Sebastian Prodinger[1,2], Raul F. Lobo[1,2] and Dionisios G. Vlachos[1,2]*

[1]Department of Chemical & Biomolecular Engineering, University of Delaware, 150 Academy St., Newark, DE 19716, USA
[2]Catalysis Center for Energy Innovation, RAPID Manufacturing Institute, and Delaware Energy Institute (DEI), University of Delaware, 221 Academy St., Newark, DE 19716, USA

* Corresponding author: vlachos@udel.edu

Keywords: Biomass, microseparator, biphasic, extraction, process intensification.

Abstract

Modular and distributed biomanufacturing requires continuous flow microreactors integrated with efficient separation units operating at comparable time scales: biphasic reactive extraction of 5-hydroxymethyl furfural (HMF) by fructose dehydration is an excellent example. The liquid-liquid extraction (LLE) and fast reaction kinetics in biphasic microchannels can immensely benefit from a downstream microseparator enabling separation of an HMF-rich organic extract and an aqueous raffinate. Here we demonstrate the successful implementation of an effective slit-shaped microseparator for eleven organic-water biphasic systems. The microseparator successfully separates six of these over reasonable flow rates. The ratio of capillary and hydraulic pressures qualitatively rationalizes the separation performance, while a transition to non-segmented flow patterns correlates with performance deterioration. Acids and salts, integral parts of the chemistry, significantly expand the flow rates for efficient separation enabling a broader slate of organic solvents. For the MIBK/water biphasic system, we demonstrate perfect separation performance over a 16-fold variation in the organic to aqueous flow ratio. Here we also integrate the microseparator and extractive microreactor into a modular system and achieve an HMF yield of up to 93% – the highest reported fractional HMF productivity of 27.9 min^{-1} – at an ultrashort residence time of 2 s. This unprecedented performance is maintained over a 50-fold fructose concentration range and is stable with time on stream. This microseparator exhibits a ten-fold reduction in separation time and substantial energy savings over conventional decanters. As such, it holds promise for continuous process intensification and modular biomanufacturing.

Introduction

Continuous Process Intensification for Biomanufacturing

5-hydroxymethylfurfural (HMF) is a versatile platform chemical whose production at high yield from sustainable, domestic biomass can enable future biorefineries to utilize the carbon captured by photosynthesis.[1-9] The high biomass volume and its associated water content make continuous, local-to-the-source processing critical for economic viability. This chemical "plant on wheels" concept, in turn, requires the development of modular, portable systems operating at ultrashort residence times (therefore, at high temperatures).[10-12] Microchemical processes possess rapid heat and mass transfer (2-3 orders of magnitude higher than batch systems), small volumes, low economic risk, and excellent repeatability, allowing precise control of process conditions.[13-15] Such control is significant in HMF production via the acid-catalyzed hexose hydrolysis, historically plagued by low yields due to undesirable side-reactions.[16, 17]

A few single-phase microfluidic reactors have investigated HMF production, achieving a maximum HMF yield of 53%.[18, 19] We recently reported the highest-ever single-phase HMF productivity (7.5 min^{-1}, defined as the HMF fractional yield per time) in a coiled microreactor under optimized reaction conditions (473 K, *p*H 0.7), operating at a residence time of 4 s.[10] The side-reactions can be minimized by substituting the aqueous phase with organic solvents (*e.g.,* dioxane, butanol, dimethyl sulfoxide).[6, 20-26] Biphasic systems, comprising an aqueous reactive phase and an organic extraction phase, have emerged as an effective means to increased HMF yield. The HMF partition coefficient (P_{HMF}), defined at the ratio of the concentrations of HMF in the organic and aqueous phases, is a key metric for extractant selection.[16, 17] Such liquid-liquid extraction (LLE) processes are especially advantageous in microchannels due to their short diffusion lengths coupled with high interfacial areas. Interestingly, most biphasic fructose dehydration microreactor studies have been carried out using methyl isobutyl ketone (MIBK), an organic solvent of a low $P_{HMF} \sim 1$[7, 27], and reported HMF yields of >70% using HCl as the catalyst.

Shimanouchi *et al.*[28] obtained an HMF yield of 88.5% in a slug flow microreactor at 453 K and a residence time of 2 min. Brasholz and coworkers[29] also investigated the fructose dehydration in slug flow with 74% HMF yield at 413 K and 15 min. In their slug flow microreactor, Lueckgen *et al.*[30] observed 91% HMF yield at 423 K and 37 s. Furthermore, Zhou and coworkers[31] demonstrated 93% HMF yield at 453 K using a dispersed flow microreactor at 4 min. Muranaka *et al.*[32] used a phosphate saline buffer as the catalyst in slug flow and reported an HMF yield of 45% at 453 K and 8 min. 2-sec-butyl phenol has a high P_{HMF}[27, 32] of 8.7 and has been used for reactive extraction in microreactors. Muranaka *et al.*[33] reported an optimal HMF yield of 81% at 453 K and 12 min in a 2-sec-butyl phenol/water slug flow, using a phosphate saline buffer as the catalyst. In general, extractant selection has been based on intuition, but recently, we introduced a systematic framework for the selection of extractants using multiscale modeling and experimentation.[27]

Despite all this progress, little attention has been paid to the downstream separation of the organic from the aqueous phase. Continuous flow separation units, easily integrable with upstream high throughput reactors, are vital for modular manufacturing.[34] Density difference-based, continuous phase separators (mixer-settlers, centrifugal extractors, and static/agitated columns) are ineffective at a small scale due to surface forces dominating over gravity or viscous forces.[35, 36] They typically expose large areas, consume high energy and solvents, and require long residence times.[37] With this in mind and the need for distributed manufacturing, we searched for modular-based two-phase flow microseparators discussed next.

Two-phase Flow Microseparators

Even though a few gravity/density-based microseparator designs exist,[38-42] most microseparators utilize differential wetting of surfaces by the aqueous and organic phases.[15, 35, 36, 43-45] Density-based microseparators have a low throughput, long residence times for droplet coalescence and settling, and broader applicability in terms of solvents, including cases where wettability-based mechanisms may fail (*e.g,.* solvents of similar surface tension). [46] In a recent comparison of the efficacy of T-shaped microseparators, it was concluded that the gravity separator had lower throughput than the wettability-based separator even with a nine-fold increase in cross-sectional area.[40]

Several liquid-liquid microseparators utilize porous membranes for the selective transport of components through the pores. Narrow pores yield considerable capillary pressures, while throughput increases with a larger number of pores.[35, 47] For example, hydrophobic Teflon® membranes with 0.1-1 μm pores permeate the non-aqueous phase to separate water-hexane mixtures up to a flow rate of 1.2 mL/min, while 0.5 μm Teflon® membranes separate toluene-water and butyl acetate-water up to 20 mL/min, though aqueous phase (retentate) contamination (>20%) was observed.[35, 47] Better control over microseparator performance can be obtained by varying the outlet tubing lengths using a secondary hydrophilic membrane or through an integrated pressure regulator, such as a needle valve, to adjust back-pressures.[15, 48-50] In general, the membrane finite-size limits the operation to low flow rates and solid impurities can plug membrane pores.[3] Membrane-based microseparators with internal pressure regulation have been commercialized recently.[51]

Capillary arrays were used to separate gas-liquid systems and oil-water systems of high interfacial tension.[52-54] Wettability-based microscale flow splitters were developed using steel needle insertion into one outlet; the separation performance was investigated up to 2.6 mL/min. However, even at 1:1 flow ratios, the aqueous fraction was contaminated with the organic phase (>5 vol.%).[36] Phase separation was similarly demonstrated by piercing the capillary wall with a hydrophilic metallic needle to draw off the aqueous phase.[44] More recently, a phase separator with a hydrophobic Teflon® T-connector, perfluoroalkoxy (PFA) tubing, and a hydrophilic oxidized stainless steel needle was used to separate four biphasic systems with interfacial tension ranging from 1.68-49.6 mN/m at flow rates of 0.15-1.5 mL/min.[15] Rapid droplet coalescence at the needle tip was ensured *via* an overnight steel needle treatment with sulfuric acid to provide a hydrophilic oxide layer, lowering the water/air contact angle from 86 ° to 28 °. A similar T-shaped microseparator using surface-treated glass and Teflon® capillaries efficiently separated biphasic mixtures from 0 to 4.4 mL/min.[40]

A wettability-based flow separator with adjustable slits of hydrophilic and hydrophobic blocks offers control over the capillary pressure.[35, 43] Teflon® and glass materials give good performance up to 50 mL/min for water-heptane.[6] This separator was successfully used to extract Co and Ni using a Cyanex 272 solvent up to 8 mL/min.[55] The slit-shaped separator performs better than a membrane over a wider flow rate range.[35]

While some phase microseparators exist, their integration with upstream reactors for continuous modular manufacturing is rarer.[34, 56-65] A few setups have been reported. Synthesis of biaryls from substituted phenols was demonstrated by integrating two microreactors, with a membrane microseparator in between, operating under low flow rates (<1 mL/min), extracting the aqueous byproducts (catalyst poison) from the first reaction.[66] Chemoenzymatic aqueous-phase cyanohydrin formation was integrated with an organic phase (dichloromethane) protection using a commercial membrane separator.[67] Coupling of the azide-alkyne cycloaddition click reaction with continuous extraction of the copper catalyst by a chelating agent was also demonstrated using

a commercial fluoropolymer membrane operating at a maximum flow rate of 1 mL/min.[68] A modular unit comprised of a reactor and a microseparator for the manufacturing of four active pharmaceutical ingredients was demonstrated with a 20% increase in the membrane separation efficiency by adding a secondary hydrophilic glass membrane to the polytetrafluoroethylene (PTFE) membrane module.[50, 69] The synthesis and purification of methyl oximino acetoacetate was also established using continuous flow generation of nitrous acid with oxime extraction by LLE.[70]

Scope of This Work

There are several technological barriers for implementing microseparators for biorefineries. The standalone microseparator performance is, with a few exceptions, benchmarked using (nearly) immiscible solvents of high interfacial tension: these are not practical for biphasic extraction. Integrated microreactor-separators usually operate at low flow rates (*i.e.,* low productivity), incompatible with high throughput and modular manufacturing concepts. Furthermore, performance robustness and durability data are lacking. No inline microseparator downstream of the fructose dehydration reactor has been demonstrated for biomass conversion. Inlet stream compositions have been synthetic; reaction intermediates, salts, acids, and solids, such as dissolved humins, in the inlet stream of a microseparator could easily cause device failure.

We demonstrate the effectiveness of a modified slit-shaped microseparator originally designed by Gaakeer *et al.*[43] for the complex biphasic fructose dehydration system for the first time. The original microseparator and specific modifications carried out in this work are detailed in the microseparator design section below. High P_{HMF} solvents can selectively concentrate HMF, be used in low quantities, and reduce processing costs. Toward this end, we recently reported an *in silico* COSMO-RS-based computational screening followed by thorough experimental verification of predicted high-performing HMF extractants, identifying several solvents with up to an order of magnitude higher P_{HMF} than the conventional extractants reported in the literature.[27] Based on our prior comprehensive study, eleven biphasic systems of varying thermophysical properties were selected. Here, the standalone microseparator performance is investigated in detail. To our knowledge, such a numerous set of solvents of varying properties has not been screened in any microseparation system. The effects of flow patterns, acid, and salt addition on separation are evaluated, and the performance is rationalized. MIBK/water is selected for a comprehensive performance evaluation over 16-fold organic:aqueous (O:A) flow ratios. Integration and optimization of our in-house fructose dehydration microreactor with the slit-shaped microseparator are successfully carried out over a 50-fold fructose concentration range. Importantly, the robustness of the system is evaluated with time-on-stream (TOS).

Materials and Experimental Methods

Materials

The microseparator was evaluated using eleven biphasic solvent systems chosen from our work on solvent selection for HMF extraction during fructose dehydration.[27] A list of the solvents used, their purity, and supplier information is provided in **Table S1** of the Supporting Information (SI). HCl (36.5-38.5 wt.%) and sodium chloride (99%) were purchased from Fisher Scientific. ASTM-Type 1 grade deionized (DI) water (Milli-Q® Direct) was used. NE-1000 syringe pumps (New Era), 60 mL syringes (Grainger), 1/8" OD PFA tubing (Idex Health), and 1/8" OD tee with 0.05” bore (Idex Health) were used for the microseparator.

Compound Quantification and Solvent Property Characterization

The HMF and solvent concentrations were quantified using high-performance liquid chromatography (HPLC). A Waters e2695 separations module was coupled to a Waters 2414 refractive index meter and a Waters 2998 photodiode array detector. A 50/50 (v/v) acetonitrile and water mixture at 0.3 mL/min (mobile phase) was employed with an Agilent Zorbax SB-C18 250 mm column at 323 K, with the HMF concentration calculated from its 254 nm absorbance peak area at 8.8 min. The residence times and quantification for each solvent are detailed in **Table S2**.

The water content of the organic phase was measured with the Mettler Toledo V20 Karl Fischer (KF) titrator in volumetric mode. The Honeywell Fluka Composite 5 two-component titrant was used along with the Honeywell Fluka Methanol Dry as the working solvent.

The aqueous-rich and organic-rich phase viscosity was measured using a rolling ball microviscometer (AMVn, Anton Paar), with the reported value being an average of three different capillary inclination angles. The interfacial tension between the two pre-equilibrated phases was measured using the Du Nouy Ring method (KSV instruments) by measuring the force on a Pt ring as it is lifted from the interface.

HCl-catalyzed fructose dehydration reaction experiments were conducted in an in-house built liquid-liquid biphasic microreactor. The reactants and products were quantified using HPLC (Water Alliance Instruments). Fructose, formic acid, levulinic acid, HMF, and methyl isobutyl ketone (MIBK) were detected using a Biorad HPX 87H column heated to 323 K and 0.005 M sulfuric acid flowing at 0.5 mL/min as the mobile phase. Fructose, formic acid, levulinic acid, HMF, and MIBK eluted at 12.4, 17.2, 19.8, 38.5, and 50.4 min, respectively. Additional small peaks indicated negligible amounts of other condensation and degradation products, which were not quantified.

Microseparator Design

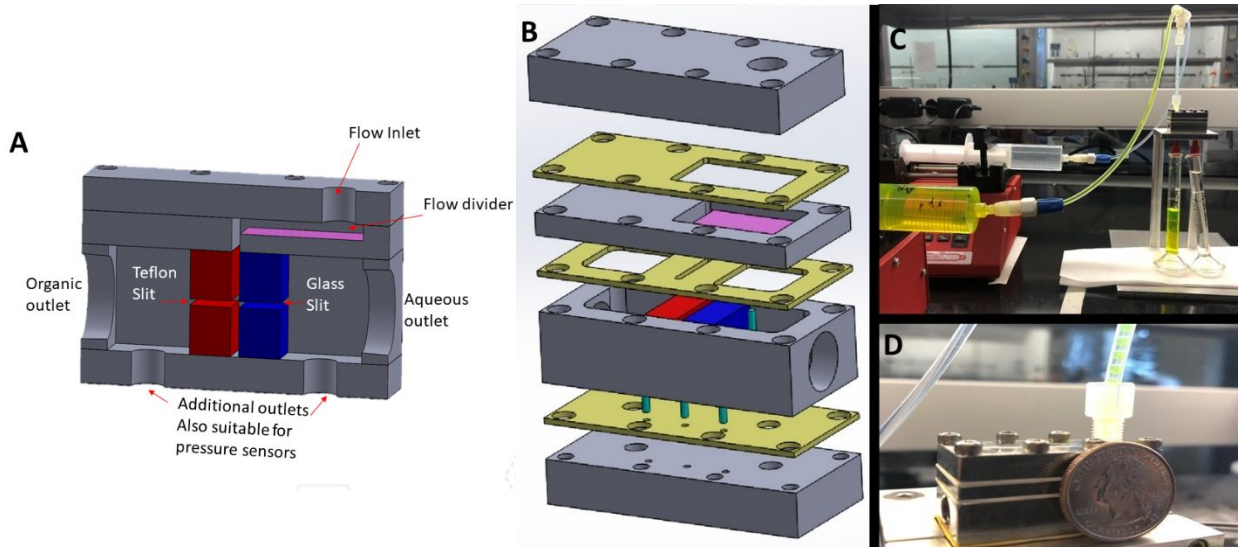

Figure 1. A) Cross-sectional view of the original slit-shaped microseparator[43], and the improved microseparator *via* **B)** substitution of glass slits by acid-treated stainless-steel and incorporation of Teflon® gaskets (yellow) in-between stainless steel blocks (grey) preventing liquid leakage, and **C)** design of a holding rig to maintain the separator horizontal as individual phases being pushed by two syringe pumps mix at the tee-junction and enter the microseparator inlet. **D)** Comparison of microseparator size to a US penny coin. The overall device dimensions are 39×18×28.3 mm.

The slit-shaped microseparator, described by Gaakeer *et al.*[43], consists of four individual stainless-steel parts (**Figure 1 A**), namely: **i)** a flow inlet to the microseparator, **ii)** a flow-divider to flatten the incoming velocity profile, **iii)** housing for the hydrophobic (Teflon®) and hydrophilic (glass) slits to separate the biphasic mixture, and **iv)** separate outlets for the aqueous and organic phases. The preferential wetting of the two slits by the solvents drives the separation, *i.e.,* the organic-rich solvent has an affinity toward the hydrophobic Teflon® slit and *vice versa*. The large fixed slit width of the design results in a low hydraulic pressure drop, which is a function of the solvent viscosity and flow rate. It can be estimated by the Hagen–Poiseuille equation (See Supporting Information). The slit height is a design variable, and narrow heights increase the capillary pressure, which is also a function of the interfacial tension and can be estimated from the Young-Laplace equation (See Supporting Information). For good separation performance, the capillary pressure must exceed the hydraulic pressure by a factor of at least two; if not, the more viscous solvent (*i.e.,* the higher hydraulic pressure) can break through the opposite slit at the same flow ratio, leading to outlet contamination.[13, 35, 43]

The slit-shaped microseparator was fabricated at the University of Delaware Research Machine Shop; its dimensions are reported in **Figure S1**. However, initial experiments led to inconsistent performance due to fluid seepage in-between the four stainless steel blocks and unsatisfactory separation performance due to the microseparator orientation. To ensure reproducible and high performance, 1/32 inch Teflon® gaskets in-between stainless-steel layers were added, and a holding rig was designed to maintain the microseparator horizontal (**Figure 1 B-C, S1**). Design specifications of the holding rig are detailed in the Supporting Information. Better performance was observed upon substitution of the fragile glass slits with stainless steel slits.[15] For satisfactory performance, fresh stainless steel slits with 1.5 mm slit height were used after treated with 98% H_2SO_4 overnight. The improved microseparator with these three modifications is shown in **Figure 1D**.

Evaluation of Microseparator Performance

For evaluating the microseparator performance, we adopted the following methodology (**Figure S2**). Pure organic solvent and water (spiked with 1 g/L HMF and 0.3 g/L fluorescein dye, used for visualization) were pre-equilibrated overnight with stirring (**Figure S2A**), and the resulting phases were separated using a separatory funnel (**Figure S2B, C**). For emulsion forming systems, centrifugation was carried out for phase separation. The resultant organic-rich and aqueous-rich equilibrated phases were loaded into separate 60 mL syringes and independently pumped (1:1 flow ratio) using syringe pumps (NE-1000, New Era) (D) through a 1/8" OD (1.5 mm ID) PFA tube. The two inlet phases meet at a tee-junction generating a biphasic flow fed into the microseparator. Having pre-equilibrated phases allows quantification of performance independent of mass transfer effects. The phase compositions at the two microseparator outlets (**Figure S2E**) were visually inspected, homogenized with acetonitrile (1:1 volume ratio), and quantified using HPLC and the KF titration, as detailed above for the water content in the organic phase. While visual inspection is a crude quantification method; still, it is quite useful to complement analytical measurements. The separator outlet compositions were compared to the equilibrated inlet phases to assess the separator performance. Both outlets of the microseparator were kept open to the atmosphere during performance evaluation to exclude any effect of downstream pressure disturbances, following the experimental design of Gaakeer *et al*.[43]

Room Temperature HMF Partitioning for Extraction

3 mL of a 1 wt% aqueous HMF solution and an equal volume of the organic solvent were mixed in a 25 mL scintillation vial with stirring at 700 rpm for 3 hr at room temperature (298 K). To determine the effect of acid and salt addition on the HMF partition coefficient (P_{HMF}), a 0.25 M HCl aqueous solution with or without 20 wt% NaCl was also added. After mixing, centrifugation was used to separate the two phases, and the collected samples were analyzed to determine the partition coefficient *via* HPLC, from the ratio of HMF molar concentrations in the organic phase (C_A^{org}) and the aqueous phase (C_A^{aq}) (Eq. 1)

$$P_A = \frac{C_A^{org}}{C_A^{aq}} \quad \textbf{(1)}$$

Integrated Microseparator with the Fructose Dehydration Extractive Microreactor

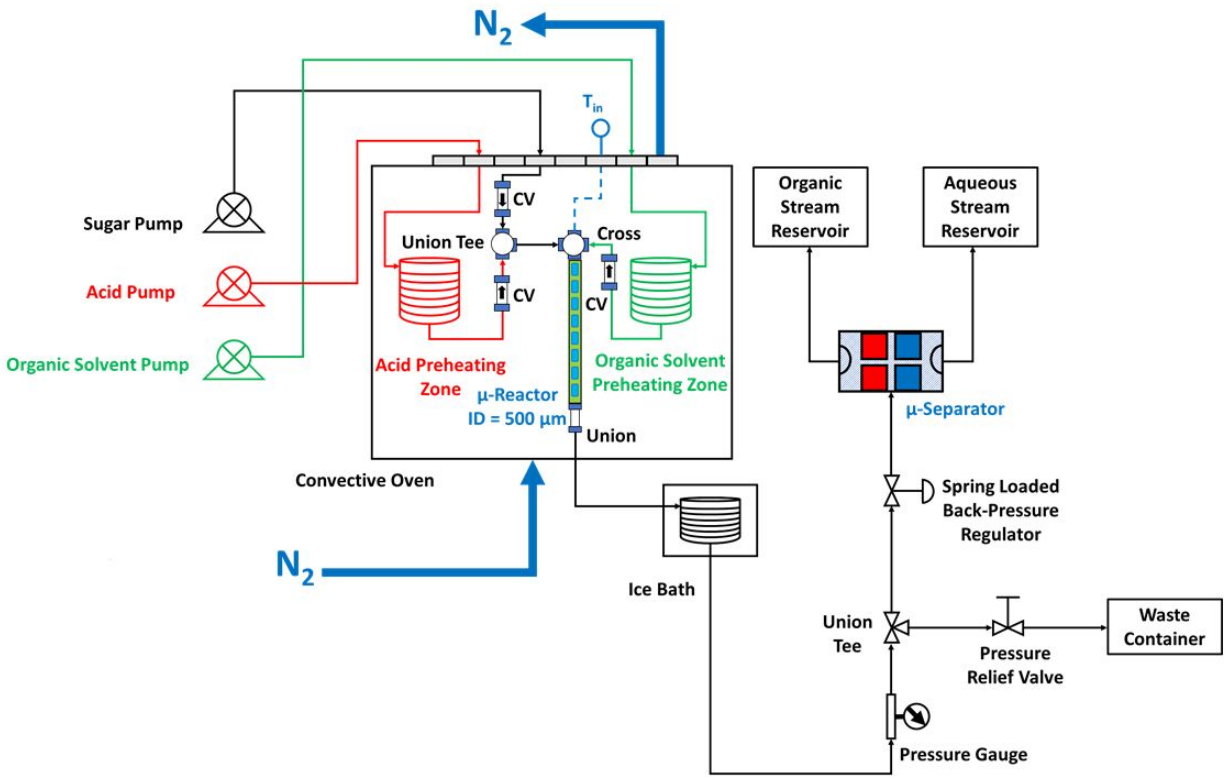

Scheme 1. Schematic diagram of the integrated microreactor/microseparator setup. The two modules can also run independently of each other. The microreactor can run a single phase or two phases (as shown here) where chemistry and extraction happen in parallel.

Scheme 1 shows a schematic of the integrated microsystem consisting of a liquid-liquid biphasic microreactor used to conduct the HCl-catalyzed fructose dehydration to HMF with simultaneous extraction of HMF from the water to an organic phase and a microseparator placed downstream. Three high-pressure piston pumps with flow rate ranges of 0.001 – 5 mL/min (Teledyne – LS Class 10), 0.01 – 10 mL/min (Teledyne – M1 Class 10), and 0.01 – 20 mL/min

pump the aqueous sugar (fructose), the acid catalyst (HCl/KCl buffer), and the organic solvent (MIBK), respectively. The internals of the acid catalyst pump are made of polyether ether ketone (PEEK), a chemically inert polymer, to prevent corrosion. In a typical experiment, the three feeds are pumped into a convection oven (Hewlett Packard GC 5890) using 1/16" PEEK (Idex Health & Science) tubing. The acid catalyst and the organic solvent are individually pre-heated to the reaction/oven temperature by flowing through 1/8" PEEK tubing (Idex Health & Science). The fructose feed line is kept short with no significant pre-heating to prevent dehydration prior to mixing with the acid and the organic solvent. Specifically, the pre-heated acid feed and the aqueous fructose feed are mixed at a 10:1 (v/v) ratio through a 1/16" PEEK union tee (Restek – 500 μm bore diameter) such that, upon mixing, the resulting aqueous mixture is only ~6 K lower than the oven temperature at the highest flow rate considered. This aqueous stream rapidly comes in contact with the pre-heated organic solvent stream in an opposed flow configuration inside a 1/16" PEEK cross connector (Restek – 500 μm bore diameter), where biphasic flow patterns form before the microreactor. An inline check valve (CV) made of PEEK (Idex Health & Science) is placed at the inlet of the fructose stream. The acid feeds into the union tee, and the organic solvent feeds into the cross connector to prevent back-flow. A 500 μm stainless steel K-type thermocouple (Omega Engineering) is inserted in the cross connector middle-top port to monitor the inlet reactor temperature. The tip of the thermocouple probe is coated with Teflon® tape to prevent corrosion and to ensure accurate temperature readings. The inlet temperature of the microreactor was that of the oven, enabling isothermal reactor operation.

The biphasic mixture flows through the microreactor, made of a 1/16" PEEK tubing (Idex Health & Science – 500 μm inner diameter) where the fructose dehydration and HMF extraction occur. Low-pressure in-house nitrogen (N_2) gas continuously purges the oven and prevents the accumulation of the organic solvent vapors in the case of leaks. The product leaves the microreactor through a 1/16" PEEK union, outside the furnace, connected to a coiled 1/16" PEEK tubing placed in an ice bath to quench the reaction quickly. A 500-psi inline PEEK back-pressure regulator (Idex Health & Science) mounted with a pressure gauge (Grainger) is used to pressurize the microreactor and maintain the biphasic mixture under subcooled conditions. A 1/16" PEEK union tee (Idex Health & Science) is coupled with a PEEK shut-off valve (Idex Health) to serve as a pressure relief mechanism and release the microreactor contents into a waste reservoir. In the cold and unpressurized section downstream of the back-pressure regulator, the product mixture flows through a translucent 1/8" PFA tubing (Idex Health & Science – 1/16" inner diameter) for optical visualization of the flow patterns before entering the microseparator. In the separator, the two solvent streams are separated and collected in two 10 mL graduated cylinders at the stainless steel and Teflon® outlets. The collected streams are analyzed using HPLC and KF analysis to quantify the concentrations and assess performance.

Results and Discussion

Standalone Microseparator Performance of Eleven Organic-Water Biphasic Systems

The water-heptane system is used for performance standardization of the slit-shaped microseparator in the literature.[43] In our case, HMF extraction from the aqueous phase to the organic phase dictates the solvent selection. Eleven organic solvents were chosen based on our previous work on HMF selective extraction[27] (**Table S1**). These solvents form biphasic systems, are thermally stable, do not react with reactants and products, and belong to select homologous series suitable for extraction (P_{HMF}>1). Their HMF partition coefficient at room temperature varies from low, e.g., ~1 (MIBK) to high, i.e., ~25 (2-chlorophenol). The water solubility in the organic

phase at room temperature varies by order of magnitude, from 2 wt% for MIBK to 19.7 wt% for 1-butanol, with best-HMF separating solvents having a higher affinity for water.[27]

The viscosity and water-solvent interfacial tension were measured (see data in **Table S2**), as these two properties are crucial for operation. We organize this information in **Figure 2A** and discuss it next. MIBK, ethyl acetate, 2-pentanone, and 2-methyl tetrahydrofuran (2-MTHF) have a lower organic-rich phase viscosity than the aqueous-rich phase (~1 cp), implying that the aqueous-rich phase at sufficiently high flow rates and a 1:1 phase flow ratio would break through the Teflon® slits overcoming capillary forces and limiting the operational space to slower flows. High interfacial tension extends the maximum flow rate due to the increased capillary forces. The interfacial tension of 2-sec-butyl phenol and MIBK is relatively high. In contrast, benzyl alcohol, 2-chlorophenol, and m-cresol are below the detection limit, foreboding non-optimal microseparator performance, consistent with emulsion formation in these systems. **Figure 2A** compares all biphasic systems against the ideal water-heptane system. All solvents have a higher viscosity and lower interfacial tension than heptane (red circle). Nine of them have an order of magnitude lower interfacial tension than the near-immiscible heptane-water system. Therefore, this work focuses on realistic solvents that possess partially soluble phases, widely varying viscosities, and low interfacial tensions. Combined, these properties, dictated by the extraction of interest, pose inherent challenges for microseparation.

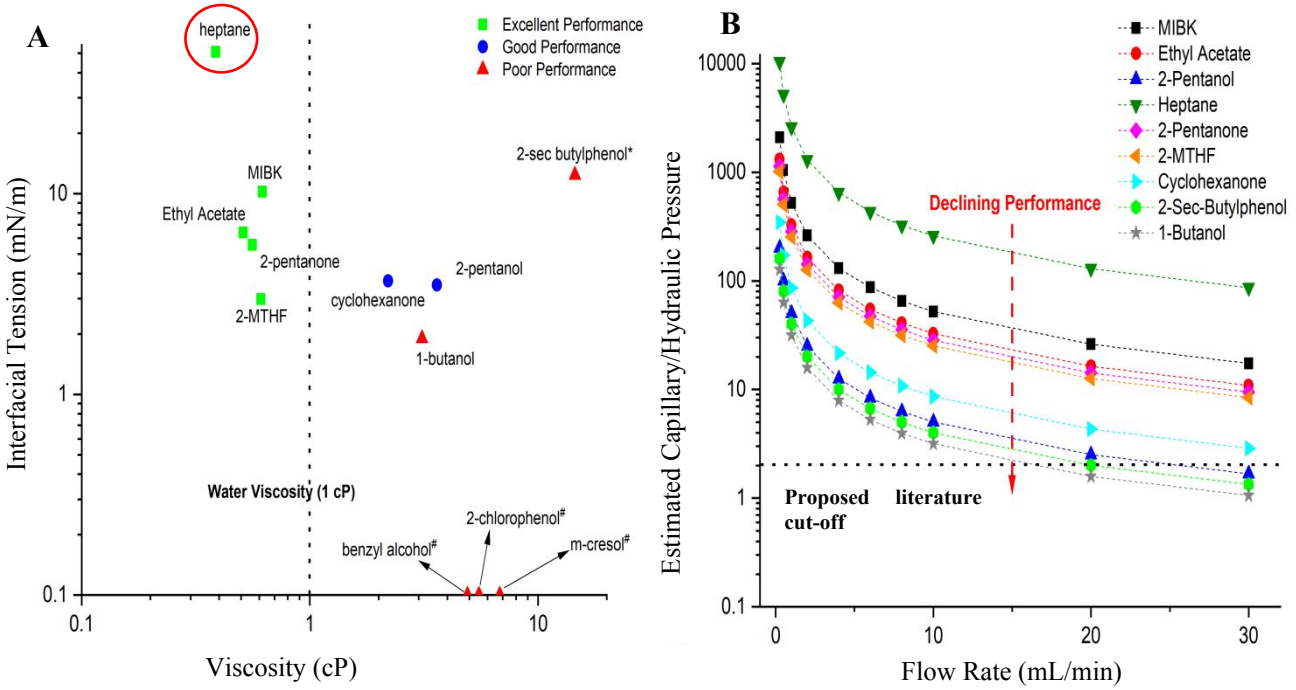

Figure 2. **(A)** Classification of the eleven organic solvents in terms of their viscosity and the interfacial tension between the aqueous-rich and organic-rich phases measured herein. Experimentally determined viscosity and interfacial tension of pre-equilibrated biphasic systems compared to the ideal water-heptane system (red circle). The viscosity of water (1 cp) is shown as a reference.
Color-coding of solvents: Excellent performance implies perfect separation across 1-15 mL/min total flow rate, good performance implies perfect separation across part of the 1-15 mL/min total flow rate, while poor performance implies no separation even at the lowest 1 mL/min flow rate. **(B)** Ratio of the theoretically estimated capillary to hydraulic pressure as a microseparator performance indicator for solvent selection. Details of the calculations are given in the SI. The ideal heptane-water system is also shown (top green triangle set of points). The dotted line indicates the

proposed literature cut-off of 2 for good microseparator performance, as a guide; we evaluate performance goodness below. Lines are guides to the eye.
#Systems with undetectable interfacial tension (interfacial tension of 0.1 mN/m^2 used as a placeholder for visualization)
*Measured viscosity outside calibrated viscometer range (till 10 cP).

The visual performance of the microseparator at 1:1 O:A ratio is shown in **Figure 3**. Excellent performance with complete phase separation is achieved in the range of 1-15 mL/min for MIBK, ethyl acetate, 2-pentanone, and 2-MTHF – these have lower organic phase viscosities than water and relatively high interfacial tensions (green points in **Figure 2A**). This combination of properties coupled with a high partition coefficient is desirable. Interfacial tension alone cannot predict performance, as evidenced by 2-pentanol and cyclohexanone possessing higher interfacial tension than 2-MTHF. Their relatively higher viscosity (blue points in **Figure 2A**) constrains the maximum flow rate to 8 mL/min (2-pentanol) and 12 mL/min (cyclohexanone), above which the organic phase breaks through the aqueous outlet.

The six solvents (green and blue points in **Figure 2A**) perform excellently up to a specific flow rate and are investigated further below. The microseparator fails to separate the other five systems, even at the lowest examined flow rate of 1 mL/min. The poor-performers (red points in **Figure 2A**) include three emulsion-forming systems with undetectable interfacial tension (benzyl alcohol, m-cresol, and 2-chlorophenol), the solvent with the lowest experimentally measurable surface tension (1-butanol), and the highest quantifiable viscosity solvent (2-sec-butyl phenol). Interestingly, the microseparator yields a pure organic phase (up to 6 mL/min) for 1-butanol and near-pure aqueous phases (up to 6 mL/min) for 2-sec-butyl phenol and 2-chlorophenol. Difficulty in the accurate visual estimation of each constituent phase of these emulsions is reflected in significantly larger measurement errors in **Figure 3.** In such cases where the wettability-based separation methods fail, density-based microsettlers may offer a possible alternative.

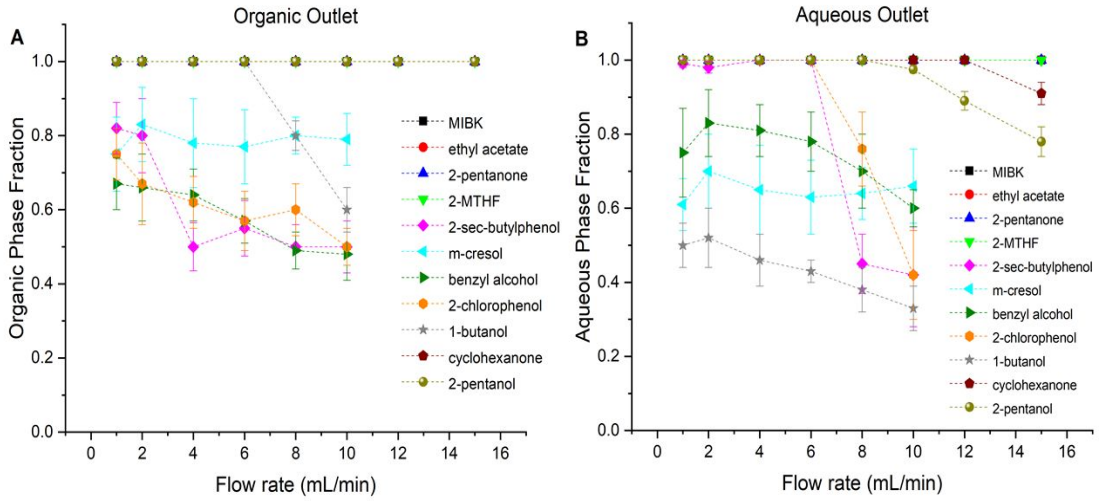

Figure 3. Visual-based microseparator performance at the **A)** organic outlet and **B)** aqueous outlet for 1:1 O:A flowrates for eleven solvents. Perfect separation occurs when the organic and water phase fraction in the corresponding outlet is 1. The data points for 6 of the 11 solvents collapse at low flow rates at a value of 1 for the organic stream. More solvents deviate from 1 in the aqueous stream. The poor performing solvents give non-perfect separation even at low flow rates.

The separation performance for these six solvents (**Figure 4, S3**) was estimated from the deviation of the outlet phase concentrations (in terms of HMF and solvent) from the equilibrium inlet concentrations *via* HPLC. Indeed, both HMF and solvent concentrations match those of the equilibrated inlet phases for 4 of the 6 systems (represented in **Figure 4** by MIBK), implying perfect separator performance. The HMF and solvent concentration patterns in the organic-rich (or aqueous-rich) phase mirror each other as expected (i.e., blue and black lines and red and green lines, respectively). Deviations from equilibrium for the organic solvent in the aqueous phase outlet occur at 10 mL/min for 2-pentanol and 15 mL/min for cyclohexanone, confirming the visual results of **Figure 3.** KF titration for the organic phase's water content agrees well with the pre-equilibrated organic phase inlet for all solvents across the flow range (1-15 mL/min). All deviations from equilibrium observed by HPLC and KF measurements are within the instrumental and experimental errors, indicated by the error bars.

For the MIBK/water biphasic system, we conducted maximum flow rate tests at 1:1 and 1:2 flow ratios complemented by KF analysis of the organic outlet stream (**Figure S4)**. Perfect separation is achieved up to 20 mL/min without HCl addition. Therefore, operating at or near these limiting conditions will result in higher HMF productivity.

In summary, the microseparator can effectively separate the two phases over a wide range of operating flowrates for six systems (2-pentanol, MIBK, 2-pentanone, ethyl acetate, 2-MTHF, and cyclohexanone). In contrast, it performs unsatisfactorily for five systems (1-butanol, m-cresol, 2-chlorophenol, benzyl alcohol, 2- sec-butyl phenol). Clearly, high viscosity, low interfacial tension, and emulsions limit the application of the microseparator. We discuss how to overcome these challenges below.

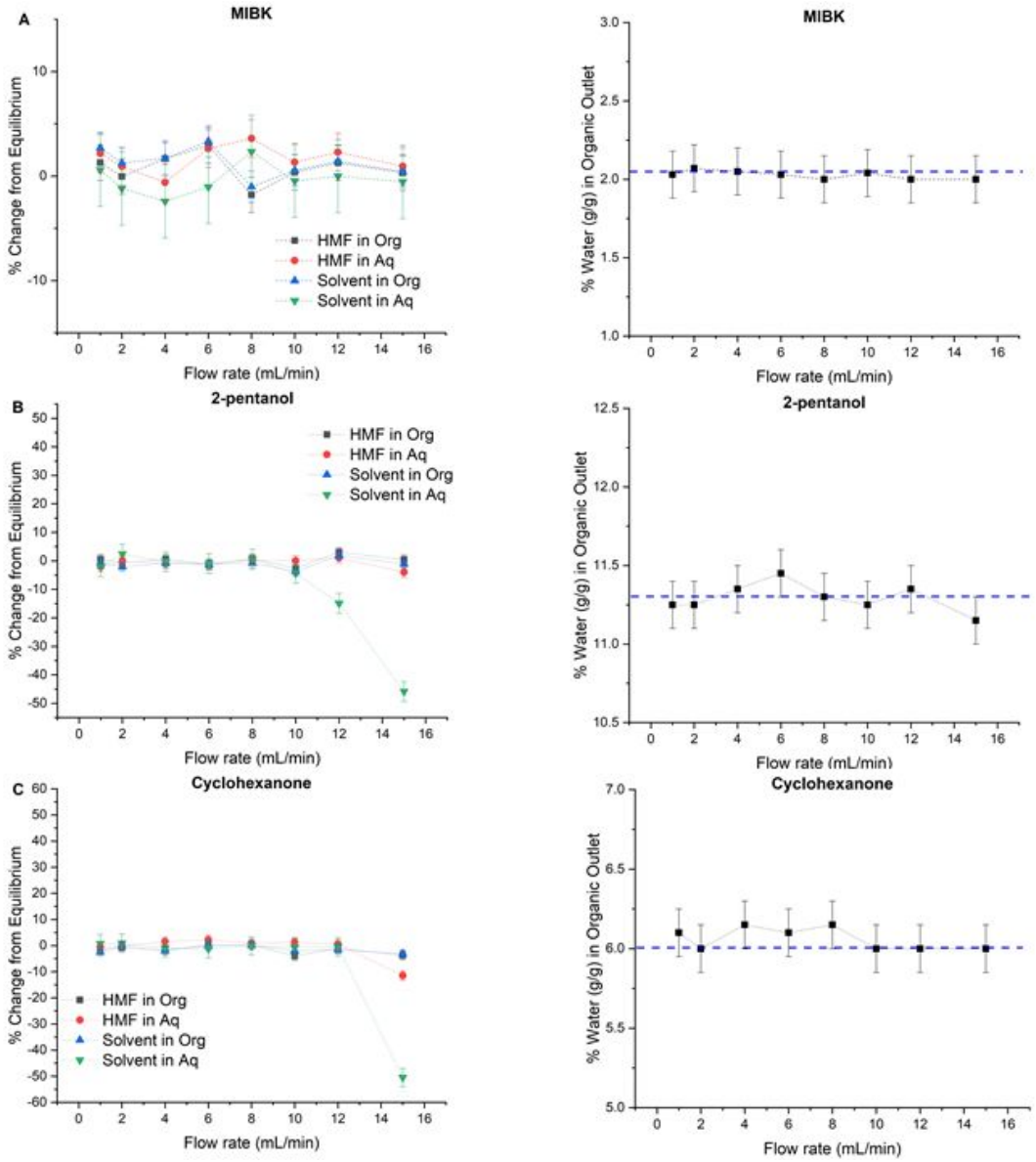

Figure 4. HPLC quantification of HMF and solvent concentration deviation at the microseparator outlets from the pre-equilibrated inlet phases for **A)** MIBK, **B)** 2-pentanol, and **C)** cyclohexanone with the corresponding organic phase water content (KF) across a 1-15 mL/min flowrate range with 1:1 flow ratio. Dashed blue lines indicate equilibrium water content in the organic phase. Error bars represent the total sampling and instrumental error.

Extending the Microseparator Operating Limits

Next, we investigate the underlying mechanisms of microseparator performance and explore extending its working limit for difficult-to-separate systems. The ratio of capillary pressure (a function of the interfacial tension) to the hydraulic pressure (a function of the viscosity and flow rate) has been employed to predict the slit-shaped microseparator performance; a value of 2 or greater has been proposed in the literature to indicate good separator performance (for the near-immiscible heptane-water system).[43] A solvent with a higher ratio performs qualitatively better, with no breakthrough of either phase through the opposite outlet and perfect phase separation.

Visual inspection of collected outlet phases is usually employed to assess the separator performance in the literature. At low ratios, we either form an emulsion (*i.e.,* a low interfacial tension) or the solvent with the higher viscosity (*i.e.,* a higher hydraulic pressure) overcomes the capillary pressure and breaks through the opposite slit, leading to imperfect phase separation and contamination of the outlet stream.

These pressures here are estimated using the Young-Laplace and the Hagen–Poiseuille equations following previous literature.[43] The ratio for eight solvent systems (except the three with no detectable interfacial tension) and the water-heptane system is shown in **Figure 2B**. MIBK has the highest ratio, followed by ethyl acetate, 2-pentanone, 2-MTHF, cyclohexanone, 2-pentanol, 2-sec-butyl phenol, and 1-butanol. The microseparator fails for the other two solvents, in qualitative agreement with the theoretical predictions.

For the six solvents separated under suitable flow rates, we discovered that the microseparator inlet flow patterns correlate strongly with the flow rate cut-off, i.e., the maximum flow rate above which the separation is imperfect. Segmented, *e.g.,* slug, flows result in a good performance; a transition to the non-segmented regime with increasing flow rate coincides with the onset of diminished performance. For example, the respective flow pattern transition (*e.g.,* 25, 10, and 15 mL/min for MIBK, 2-pentanol, and cyclohexanone, respectively; see **Figure S5**) and the cut-off for perfect separation (**Figure 3**) correlate strongly. Similar observations hold for the other three solvents (figure not shown). The transition occurs at a solvent-specific flow rate due to their different thermophysical properties.[71] Segmented flows are maintained at higher flow rates for high interfacial tension solvents, such as MIBK. These observations are consistent with the literature reporting an excellent slit-shaped microseparator performance for slug flows.[43] Even though not pursued here, the integrated system throughput can be further enhanced by operating at higher flow rates and increasing the microreactor length to maintain the optimal reaction time while enlarging the inner diameter of the inlet tubing of the microseparator to fine-tune segmented flows, enabling shorter separation times.[35, 71]

Surface modifications of slits or the use of other make-materials can introduce super-hydrophilic and hydrophobic surfaces to enhance microseparator performance.[15, 35, 40] Here, we report an alternative, simple synergistic approach to significantly improve the performance of otherwise inseparable biphasic systems: the effect of salt (NaCl) and acid (HCl), components integral to fructose dehydration.[72] Favorable HMF production requires low *p*H (<1), using strong acids and/or buffer solutions containing salts.[10, 73] Several studies noted the favorable effect of salt on HMF partitioning into the organic phase in biphasic systems and reduced solubility between solvents.[3, 8]

Here we leverage the fact that beyond affecting the extraction in the reactor, salts also enhance interfacial tension and cause de-emulsification, important aspects for the microseparation. We also expect that the segmented flow patterns are maintained over a broader range of flow conditions.[71] Therefore, salt or acid addition is likely to affect the overall HMF production and separation synergistically. Indeed, our room temperature HMF partitioning studies, with 0.25 M HCl (*p*H 0.7) and 20 wt% NaCl addition, demonstrate significant enhancements (**Figure S6**) for 10 of the 11 biphasic systems (except m-cresol), with the highest increase in partitioning for cyclohexanone (94%) and benzyl alcohol (72%). Significantly, KF analysis indicates a "salting-out" effect: significantly decreased phase miscibility for all biphasic systems (**Table S3**), an indication of increased interfacial tension (properties not measured experimentally).

1-butanol, m-cresol, and 2-chlorophenol forming inseparable biphasic systems were selected to investigate the effect of acid and salt on microseparator performance (**Figure 5)**. The first has

the lowest measurable interfacial tension; the other two form stable emulsions without phase separation over 48 hr. HCl added to the 1-butanol-water system (**Figure 5A**) decreases the organic-rich phase breakthrough in the aqueous outlet. With 20 wt% NaCl and HCl added, the microseparator separates the butanol-water up to 8 mL/min, an unprecedented improvement over the base case, where even a flow of 1 mL/min cannot be separated.

Unlike 1-butanol (P_{HMF} =1.5), emulsion-forming solvents (m-cresol, 2-chlorophenol) have an order of magnitude higher HMF partition coefficient, *e.g.,* P_{HMF} = 25.9 using 2-chlorophenol. Therefore, successful phase separation of such biphasic systems is vital. The HCl addition leads to visual phase separation within 5 min (**Figure S7**); NaCl and HCl result in a perfect separation up to 4 mL/min. Salt addition also significantly enhances P_{HMF} for 2-chlorophenol by 57% to 40.8, highlighting synergistic salt effects on phase separation and HMF partitioning.

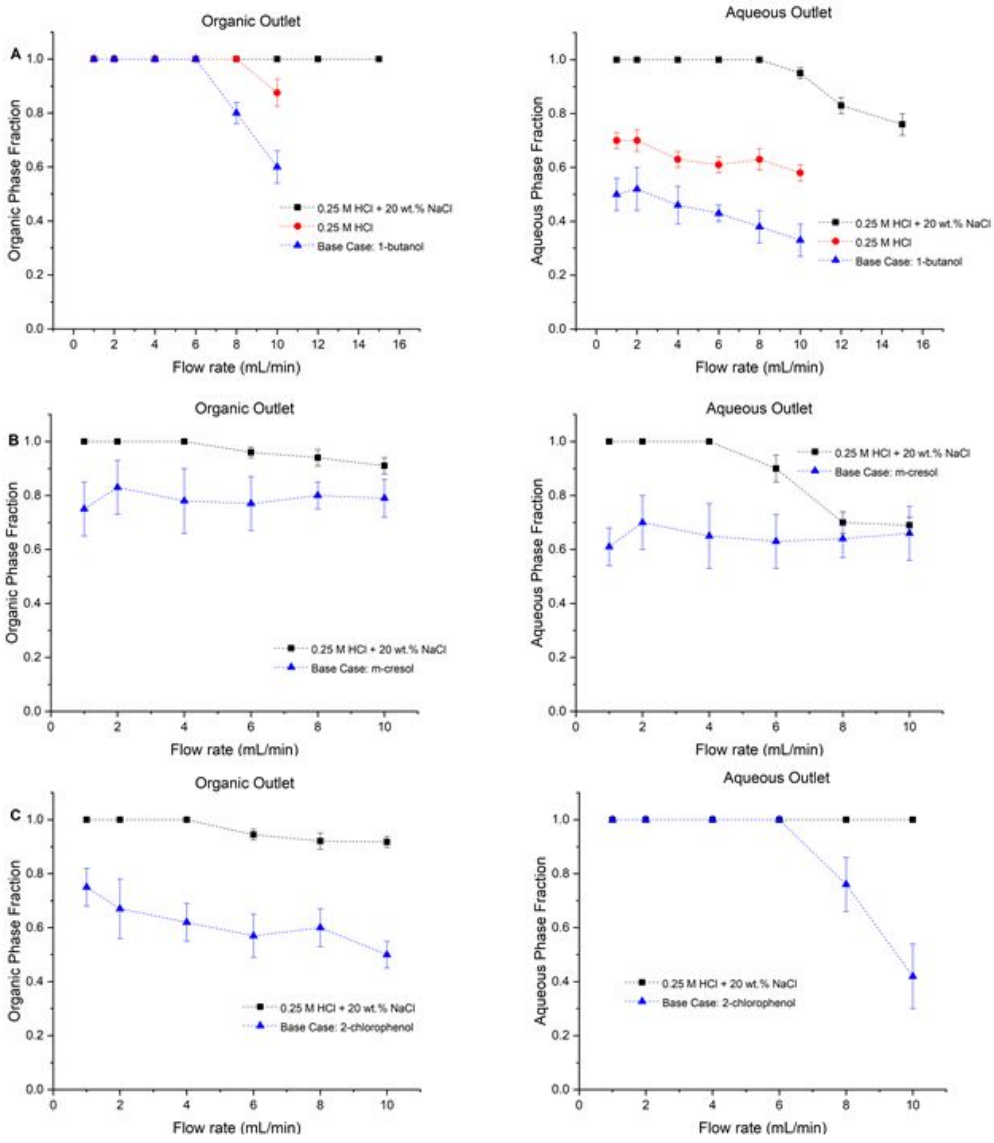

Figure 5. Effect of additives (0.25 M HCl & 20 wt% NaCl) on the microseparator performance for **A)** 1-butanol**, B)** m-cresol, and **C)** 2-chlorophenol.

Lastly, we study the effect of the O:A ratio on the microseparator performance using the MIBK/water biphasic mixture (Figure S8), which produces high HMF yields in microreactors. Visually, the microseparator achieves complete phase separation of the biphasic system at the flow ratios investigated from O:A = 1:4 to 4:1 (data not shown). HPLC and KF analysis of the separator outlets (**Figure S8**) corroborate the visual observations giving compositions quantitatively similar to the inlet over this broad (16-fold) aqueous to organic flow ratio variation, showcasing the versatility and large operating regime of the microseparator.

Integration of Microseparator with the Fructose Dehydration Reactor

We further investigate the HCl-catalyzed fructose dehydration to HMF in a MIBK/water biphasic microreactor integrated with the microseparator downstream. To our knowledge, this is the first reactive separation plus separation integrated microsystem for modular biorefineries. The biphasic microreactor operates at the optimal reaction temperature and catalyst (HCl/KCl buffer) concentration from our previous work, where the highest HMF yield of 54% was reported in a monophasic aqueous microreactor at an ultrafast residence time (τ) of 4 s.[10] We further optimize the biphasic system below.

Figure 6A and **B** plot, respectively, the reactivity (exit of the extractive microreactor) and the weight percent of water in the MIBK phase collected at the outlet (microseparator performance metric) vs. the residence time of the microreactor, at an O:A ratio of 1:1. Four characteristic biphasic flow patterns are seen in the reactor, namely slug, droplet, parallel, and annular as τ varies. At the inlet of the microseparator, the flow patterns become segmented flows (slug and slug-drop flow) as the biphasic mixture entered the 1/8" PFA tubing. This change in flow patterns between the integrated system components underscores our hypothesis above that one can tune the flow patterns. In fact, one could optimize relatively independently the flow patterns in the microreactor for mass transfer and the microseparator, e.g., to slug, for separation, by simply changing the microcomponent diameter.

The fructose conversion monotonically increases with increasing residence time up to 100% at τ = 2 s. At the same residence time, the HMF yield reaches a maximum of 86%, highlighting the fact that the MIBK/water biphasic system enables higher throughput for HMF production by reducing the optimal residence time 2-fold and simultaneously increasing the HMF yield by 60%, relative to the monophasic aqueous reactor. Longer residence times show significant HMF degradation with the rehydration products (levulinic acid and formic acid) reaching 40% at τ = 30 s, with the carbon balance steadily dropping due to the formation of humins. Control of residence time, enabled at the microscale, is essential to achieve high productivity. Excitingly, downstream inline integration of the microseparator leads to perfect visual phase separation of the phases. For all residence times, the water concentration in the MIBK phase at the microseparator outlet does not significantly differ from that obtained with the standalone biphasic microreactor where the two phases are separated by decantation, suggesting equilibrium with perfect separation by the integrated system.

Since HMF shows poor partitioning in the MIBK/water system (P_{HMF} =1), O:A ratios >1 are typically required to improve the HMF yield. **Figure 6C** and **D** present the experimental data for increased O:A ratio at τ = 2 s. The fructose conversion and the levulinic acid and formic acid yields remain unaffected while changing the O:A ratio; the HMF yield and the carbon balance exhibit a maximum at an O:A ratio of 2:1. Under these conditions, the HMF yield improves to 93% with a carbon balance of ~98%, that is, minimal humins formation.

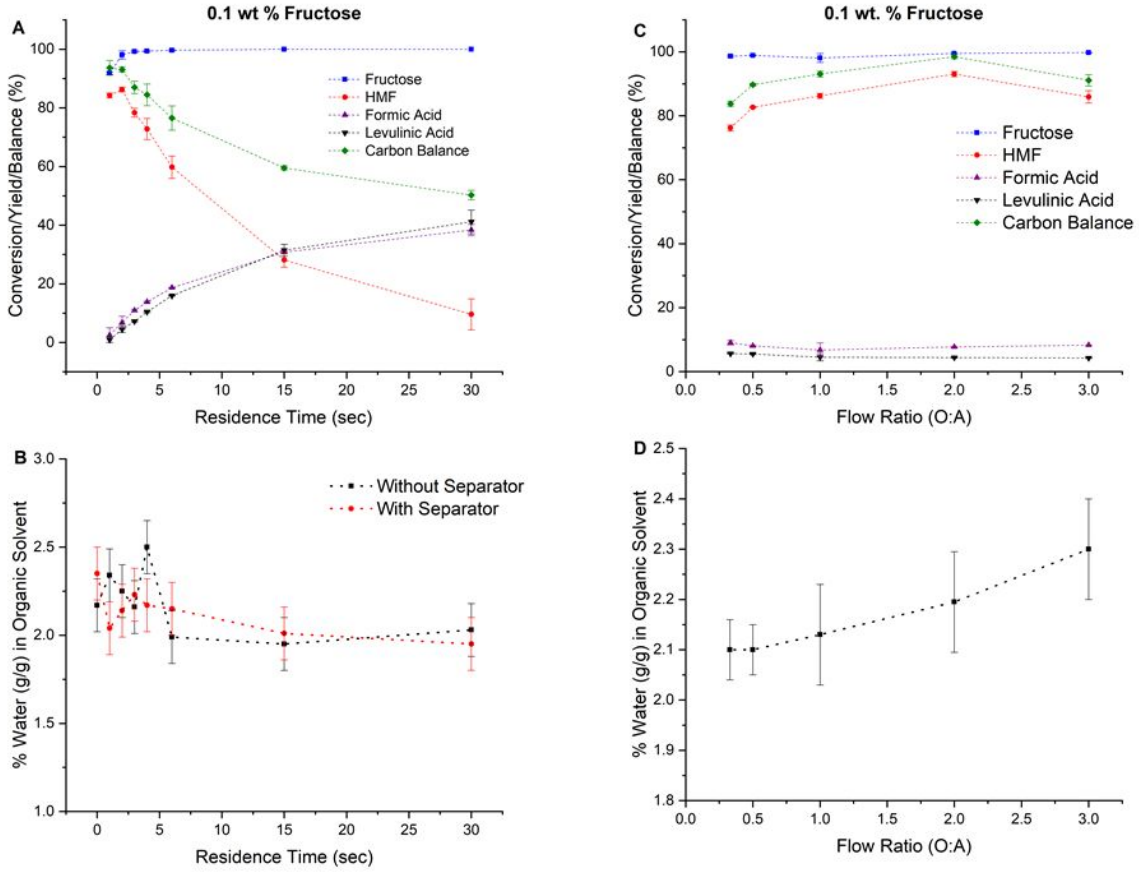

Figure 6. Effect of **A)** residence time at 1:1 MIBK/aqueous phase flow ratio and **C)** flow ratio at a residence time of 2 s on the yields, conversion, and carbon balance of the fructose dehydration reaction at *p*H 0.7, 473 K at 0.1 wt% fructose loading. Corresponding organic phase water content **(B, D)** at the integrated microseparator outlet, including comparison without microseparator **(B).**

Given the importance of achieving high HMF productivity, we assessed the integrated process performance at high fructose loadings. Our results (**Figure 7A**) show high HMF yields over a large concentration range (50-fold increase in fructose inlet concentration) with excellent separation (visual; data not shown); corroborated by KF analysis of the water content at the organic outlet (**Figure 7B**). The gradual darkening of the organic outlet streams (**Figure S10A**) reflects higher HMF concentrations, whereas the aqueous phase is considerably clearer than the organic phase (**Figure S10B**).

Time-on-stream Performance of the Microseparator and the Integrated System

These encouraging results prompted us to study the time-on-stream (TOS) of the microseparator performance over a 60 hr timeframe at low flow rates (0.2 mL/min) using a MIBK/water 1:1 flow ratio system. The outlet streams were collected and homogenized to analyze the average compositions using KF titration (**Figure S11**). The results demonstrate robust operation of the microseparator over 60 hr without apparent fouling or performance deterioration.

Further TOS studies of the integrated system were conducted. High HMF yield (>93%) and C balance (>98 %) were maintained over 2 hr, along with excellent visual separation (data not shown). Interestingly, the amount of water in the organic stream from the separator outlet at 5 wt%

fructose concentration was nearly 4%, much higher than the 2% observed for the two-component MIBK/water biphasic system at lower fructose loadings (**Figure 7B**). Analysis without the microseparator leads to similar results (**Figure 7D**). The multicomponent nature of the fructose dehydration system is responsible for this effect. Similarly, the HMF partition coefficient is ~50% higher in the actual reaction system. The separator performance fluctuates initially but stabilizes after about 30 min and gives perfect separation performance. These results unequivocally confirm the practicality of our integrated setup for modular HMF manufacturing with unprecedented productivities. They also point that actual streams are essential for evaluating system components.

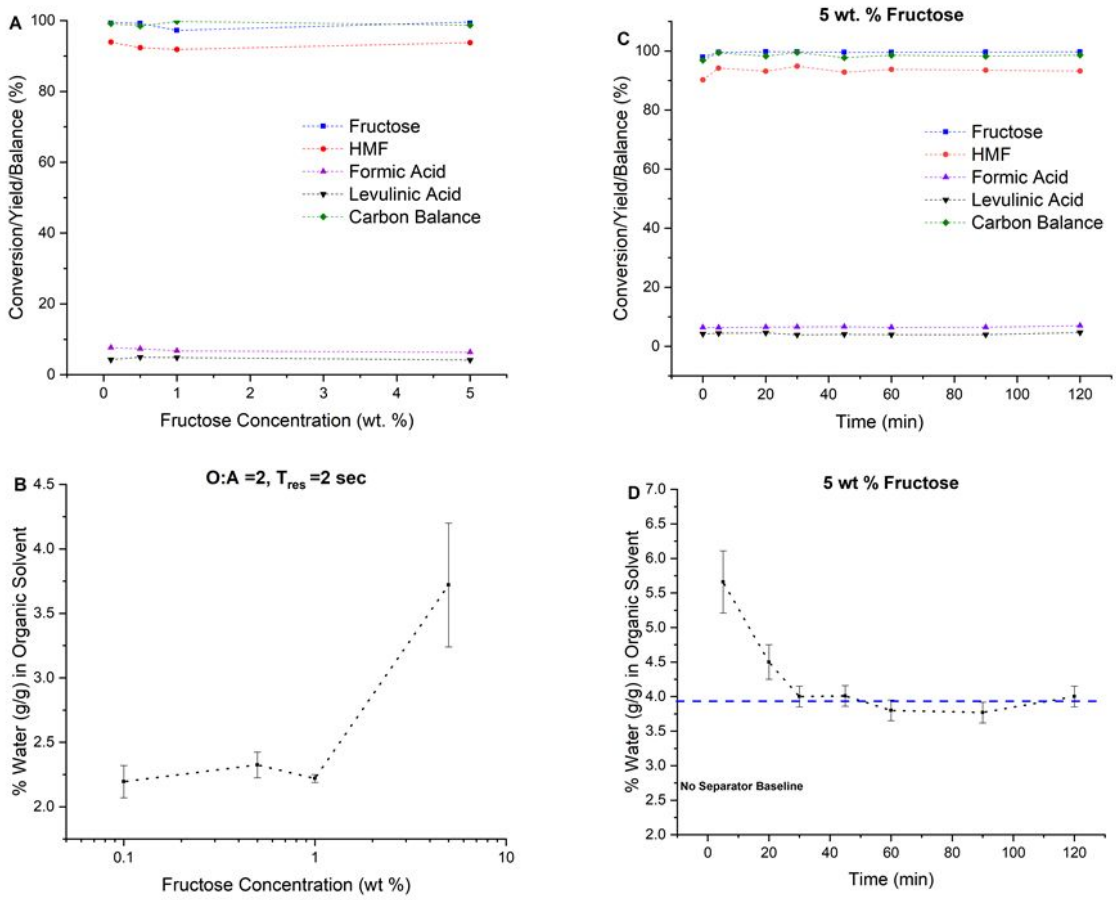

Figure 7. Effect of **A)** increasing fructose concentration, and **C)** time on stream runs at 5 wt% fructose on the yield, conversion, and carbon balance of the fructose dehydration reaction at pH 0.7, 200 473 K at a residence time of 2 s and O:A =2. Corresponding organic phase water content **(B, D)** at the integrated microseparator outlet for both cases. The blue dashed line in **(D)** denotes the equilibrium water content.

Process Intensification and Energy Savings

An important metric for microseparator performance is its separation time, *i.e.,* the residence time in the microseparator. Experimentally, the dead volume of the microseparator was determined at two different flow rates as ~0.6 mL (**Table S4**), resulting in a residence time of 36 s at 1 mL/min flow rate. The following empirical equation is used to estimate the separation time of clean, non-

emulsion forming liquid phases in gravity decanters, the simplest and widely used industrial phase-separator[74]

$$t = 100\frac{\mu}{\rho_a - \rho_b} \quad \textbf{(2)}$$

where t is the separation time (hr), ρ is the density of a liquid phase (kg/m^3), and μ is the viscosity of the continuous phase (cP) (**Figure S13**). For the water-MIBK system, this separation time is 30.3 min. For lower density differences, **Figure S8** indicates the separation times of gravity decanters are several hours. These estimates agree well with the estimated residence time of 9-60 min in conventional mixer-settlers.[75] The much longer times than the reactor residence time render a gravity settler of little practical use.

Energy-intensive and expensive centrifugal decanters (hydrocyclones) enable faster separation by employing 1000-fold or higher *g*-forces. Microseparator systems, in general, consume only 0.2-20 kJ/m^3 of liquid compared to 0.5-190 kJ/m^3 of agitated extractors, 150-200 kJ/m^3 of mixer-settler systems, and 850-2600 kJ/m^3 of centrifugal extractors, demonstrating order(s) of magnitude energy savings than conventional contactors.[14, 36] Thus, the slit-shaped microseparator has order(s) of magnitude shorter separation time (3.6 s at 10 mL/min flow rate) and lower energy consumption than traditional industrial contactors. The higher flow rates handled by the microseparator imply that one can run several reactors at the optimal residence time in parallel (scale-out) for each single microseparator or enhance the rate and reactor length to improve throughput and match time scales between the extractive reactor and the downstream splitter.

The slit-shaped microseparator developed in this work compares favorably for single-pass liquid phase separations with the lab-scale commercial microseparator (SEP-10)[51] with similar internal volume, chemical compatibility, safety, and ease of use, while achieving up to 5 times higher throughput (*e.g.,* for the heptane-water system)[43] and is amenable to long-term operation under complex process streams containing solids (*e.g.,* humins); these complex streams containing oligomers and biopolymers likely would lead to pore blockage of membranes. Unlike SEP-10, the performance of the slit-shaped microseparator has not been evaluated under pressurized conditions or high temperatures (beyond the scope of the present investigation) and is worth pursuing in future work. In general, multifold flow rate enhancement beyond the operating flow rate limit can be achieved through internal numbering up of microseparators; a multiport manifold can distribute incoming high flow rates into several flow streams, each an independent input to one microseparator operating at or below the maximum flow rate limit established in this work. In addition, use of multistage countercurrent cascades with interconnected microseparators and pumps and pressure regulators can enhance HMF extraction beyond the single equilibrium stage demonstrated here and aid in further process intensification.[46, 76, 77]

Conclusions

We demonstrated a slit-shaped microseparator for biphasic flow intensified separation and modular manufacturing of biorefineries. Modifications to a previously reported design, including Teflon® gaskets and a horizontal holding rig, enable enhanced and robust performance. Standalone evaluation of separation performance at O:A ratio of 1:1 shows excellent phase separation for six solvents (out of eleven). We discovered a strong correlation between segmented flow patterns and good separation performance and propose methods to enhance performance. The ratio of capillary and hydraulic pressures can qualitatively explain the microseparator performance. Importantly, we report that the operating regime of the microseparator is greatly enhanced by acid and/or salt addition, and even emulsion-forming solvents are amenable to phase separation at slower flow rates. This is in addition to the benefit of increasing the HMF partitioning and reducing

the organic fraction in water. Satisfactory separation performance is obtained over a 16-fold increase in flow ratio of the MIBK/water biphasic system.

The microseparator was also integrated with our previously developed extractive microreactor for fructose dehydration. We identified reaction conditions (τ =2 s, O:A =2) leading to one of the highest HMF yields (93%) maintained for a 50-fold higher fructose concentration of 5 wt% in water, with perfect separation using the integrated microseparator. TOS studies for over 2 hr and 60 hr confirmed consistent performance of the reactor-separator and the standalone microseparator respectively. A maximum separator flow rate for the MIBK/water up to 6 times higher than the optimal reactor flow rate demonstrates the potential for further productivity enhancements using microreactors in parallel (scale-out) or by increasing flow rate and reactor length. The comparable time scales of reaction and separation showcase, as our experiments demonstrate, that integration is entirely feasible. The broad operating range of the microseparator, its order of magnitude lower separation time and energy consumption compared to traditional contactors, and its successful integration with microreactors over long times could make it an integral part of modular biomanufacturing.

Associated Content

Supporting Information

List of all solvents, thermophysical properties of eleven solvent systems, measured partition coefficients and mutual phase solubilities with and without salt addition, estimation of microseparator dead volume, design dimensions of the microseparator, experimental scheme for performance evaluation, HPLC quantification and organic phase water content for ethyl acetate, 2-pentanone and 2-MTHF at 1:1 O:A ratios and MIBK across 1:4 to 4:1 flow ratios, ratio of capillary to hydraulic pressures for the solvent systems, flow patterns of solvent systems with flow rate variation, effect of acids on emulsion forming m-cresol and 2-chlorophenol systems, the integrated reactor-microseparator setup, color of different organic and aqueous phases across varying fructose concentrations, time on stream experiments for the MIBK/water system, and separation time estimates with the gravity decanter are included in the Supporting Information.

Author Information

Corresponding Author

*vlachos@udel.edu

Author Contributions

All authors wrote the manuscript and approved the final version of the manuscript.

Conflicts of Interest

There are no conflicts to declare.

Acknowledgments

This work was supported in part by the RAPID manufacturing institute via the Department of Energy (DOE) Advanced Manufacturing Office (AMO), award number DE-EE0007888-7.6. RAPID projects at the University of Delaware are also made possible in part by the State of Delaware's funding. The Delaware Energy Institute gratefully acknowledges the State of Delaware's support and partnership. We are grateful to Brian Brant (University of Delaware

College of Engineering Machine Shop) for his support in fabricating the microseparator and holding rig.

References

1. J. J. Bozell and G. R. Petersen, *Green Chem.*, 2010, **12**, 539-554.
2. M. Dusselier, M. Mascal and B. F. Sels, in *Selective Catalysis for Renewable Feedstocks and Chemicals*, ed. K. M. Nicholas, Springer International Publishing, **2014**, DOI: 10.1007/128_2014_544.
3. Y. Román-Leshkov and J. A. Dumesic, *Top. Catal.*, 2009, **52**, 297-303.
4. C. Sievers, I. Musin, T. Marzialetti, M. B. Valenzuela Olarte, P. K. Agrawal and C. W. Jones, *ChemSusChem*, 2009, **2**, 665-671.
5. T. Werpy and G. Petersen, *Top Value Added Chemicals from Biomass: Volume I -- Results of Screening for Potential Candidates from Sugars and Synthesis Gas*, Report DOE/GO-102004-1992, National Renewable Energy Lab., Golden, CO (US), **2004**.
6. A. A. Rosatella, S. P. Simeonov, R. F. M. Frade and C. A. M. Afonso, *Green Chem.*, 2011, **13**, 754-793.
7. J. N. Chheda, Y. Román-Leshkov and J. A. Dumesic, *Green Chem.*, 2007, **9**, 342-350.
8. Y. Román-Leshkov, J. N. Chheda and J. A. Dumesic, *Science*, 2006, **312**, 1933-1937.
9. K. Kohli, R. Prajapati and B. K. Sharma, *Energies*, 2019, **12**, 233.
10. P. Desir, B. Saha and D. G. Vlachos, *Energy Environ. Sci.*, 2019, **12**, 2463-2475.
11. A. Oasmaa and S. Czernik, *Energy Fuels*, 1999, **13**, 914-921.
12. A. V. Bridgewater and I. Imeche; Imeche, in *Renewable Bioenergy - Technologies, Risks and Rewards*, 2003, vol. 2003, pp. 33-61.
13. N. Assmann, A. Ładosz and P. Rudolf von Rohr, *Chem. Eng. Technol.*, 2013, **36**, 921-936.
14. M. N. Kashid, A. Renken and L. Kiwi-Minsker, *Chem. Eng. Sci.*, 2011, **66**, 3876-3897.
15. D. Liu, K. Wang, Y. Wang, Y. Wang and G. Luo, *Chem. Eng. J.*, 2017, **325**, 342-349.
16. J. Esteban, A. J. Vorholt and W. Leitner, *Green Chem.*, 2020, **22**, 2097-2128.
17. B. Saha and M. M. Abu-Omar, *Green Chem.*, 2014, **16**, 24-38.
18. T. S. Hansen, J. M. Woodley and A. Riisager, *Carbohydr. Res.*, 2009, **344**, 2568-2572.
19. T. Tuercke, S. Panic and S. Loebbecke, *Chem. Eng. Technol.*, 2009, **32**, 1815-1822.
20. B. F. M. Kuster, *Starch - Stärke*, 1990, **42**, 314-321.
21. D. Steinbach, A. Kruse, J. Sauer and P. Vetter, *Energies*, 2018, **11**, 15.
22. T. G. Bonner, E. J. Bourne and M. Ruszkiewicz, *J. Chem. Soc.*, 1960, DOI: 10.1039/jr9600000787, 787-791.
23. R. M. Musau and R. M. Munavu, *Biomass*, 1987, **13**, 67-74.
24. D. W. Brown, A. J. Floyd, R. G. Kinsman and Y. Roshanali, *J. Chem. Technol. Biotechnol.*, 1982, **32**, 920-924.
25. H. H. Szmant and D. D. Chundury, *J. Chem. Technol. Biotechnol.*, 1981, **31**, 135-145.
26. L. C. Blumenthal, C. M. Jens, J. Ulbrich, F. Schwering, V. Langrehr, T. Turek, U. Kunz, K. Leonhard and R. Palkovits, *ACS Sustainable Chem. Eng.*, 2016, **4**, 228-235.
27. Z. Wang, S. Bhattacharyya and D. G. Vlachos, *Green Chem.*, 2020, **22**, 8699-8712.
28. T. Shimanouchi, Y. Kataoka, T. Tanifuji, Y. Kimura, S. Fujioka and K. Terasaka, *AIChE J.*, 2016, **62**, 2135-2143.
29. M. Brasholz, K. von Känel, C. H. Hornung, S. Saubern and J. Tsanaktsidis, *Green Chem.*, 2011, **13**, 1114-1117.

30. J. Lueckgen, L. Vanoye, R. Philippe, M. Eternot, P. Fongarland, C. de Bellefon and A. Favre-Réguillon, *J.Flow.Chem.*, 2018, **8**, 3-9.
31. C. Zhou, C. Shen, K. Ji, J. Yin and L. Du, *ACS Sustainable Chem. Eng.*, 2018, **6**, 3992-3999.
32. Y. Muranaka, K. Matsubara, T. Maki, S. Asano, H. Nakagawa and K. Mae, *ACS Omega*, 2020, **5**, 9384-9390.
33. Y. Muranaka, H. Nakagawa, R. Masaki, T. Maki and K. Mae, *Ind. Eng. Chem. Res.*, 2017, **56**, 10998-11005.
34. I. V. Gursel, N. Kockmann and V. Hessel, *Chem. Eng. Sci.*, 2017, **169**, 3-17.
35. I. V. Gursel, S. K. Kurt, J. Aalders, Q. Wang, T. Noël, K. D. P. Nigam, N. Kockmann and V. Hessel, *Chem. Eng. J.*, 2016, **283**, 855-868.
36. M. N. Kashid, Y. M. Harshe and D. W. Agar, *Ind. Eng. Chem. Res.*, 2007, **46**, 8420-8430.
37. T. Xie, Y. Ma and C. Xu, *Chem. Eng. Sci.*, 2020, **223**, 115745.
38. S. Kumar, B. Kumar, M. Sampath, D. Sivakumar, U. Kamachi Mudali and R. Natarajan, *J. Radioanal. Nucl. Chem.*, 2012, **291**, 797-800.
39. K. Benz, K.-P. Jäckel, K.-J. Regenauer, J. Schiewe, K. Drese, W. Ehrfeld, V. Hessel and H. Löwe, *Chem. Eng. Technol.*, 2001, **24**, 11-17.
40. W. Lan, D. Liu, X. Guo, A. Liu, Q. Sun, X. Li, S. Jing and S. Li, *Ind. Eng. Chem. Res.*, 2020, **59**, 12262-12269.
41. M. Seručnik, F. A. Vicente, Ž. Brečko, J. A. P. Coutinho, S. P. M. Ventura and P. Žnidaršič-Plazl, *ACS Sustainable Chem. Eng.*, 2020, **8**, 17097-17105.
42. W.-T. Wang, F.-N. Sang, J.-H. Xu, Y.-D. Wang and G.-S. Luo, *RSC Adv.*, 2015, **5**, 82056-82064.
43. W. A. Gaakeer, M. H. J. M. de Croon, J. van der Schaaf and J. C. Schouten, *Chem. Eng. J.*, 2012, **207-208**, 440-444.
44. F. Scheiff, M. Mendorf, D. Agar, N. Reis and M. Mackley, *Lab Chip*, 2011, **11**, 1022-1029.
45. F. Strnisa, P. Žnidaršič-Plazl and I. Plazl, *Chem. Biochem. Eng. Q.*, 2020, **34**, 73-78.
46. M. Peer, N. Weeranoppanant, A. Adamo, Y. Zhang and K. F. Jensen, *Org. Process Res. Dev.*, 2016, **20**, 1677-1685.
47. J. G. Kralj, H. R. Sahoo and K. F. Jensen, *Lab Chip*, 2007, **7**, 256-263.
48. A. J. Harvie, J. O. Herrington and J. C. deMello, *React. Chem. Eng.*, 2019, **4**, 1579-1588.
49. J. H. Bannock, T. Y. Lui, S. T. Turner and J. C. deMello, *React. Chem. Eng.*, 2018, **3**, 467-477.
50. J. Imbrogno, L. Rogers, D. A. Thomas and K. F. Jensen, *Chem. Commun.*, 2018, **54**, 70-73.
51. Zaiput Flow Technologies (https://www.zaiput.com/product/liquid-liquid-gas-separators/), (accessed 4/5/2021).
52. O. K. Castell, C. J. Allender and D. A. Barrow, *Lab Chip*, 2009, **9**, 388-396.
53. A. Günther, M. Jhunjhunwala, M. Thalmann, M. A. Schmidt and K. F. Jensen, *Langmuir*, 2005, **21**, 1547-1555.
54. M. D. Roydhouse, M. Pradas, N. Al-Rifai, B. Azizi, E. H. Cao, S. Kalliadasis and A. Gavriilidis, *Chem. Eng. Sci.*, 2014, **114**, 30-39.
55. L. H. Zhang, V. Hessel, J. H. Peng, Q. Wang and L. B. Zhang, *Chem. Eng. J.*, 2017, **307**, 1-8.
56. K. Wang and G. S. Luo, *Chem. Eng. Sci.*, 2017, **169**, 18-33.

57. J. Jiao, W. Z. Nie, T. Yu, F. Yang, Q. Zhang, F. Aihemaiti, T. J. Yang, X. Y. Liu, J. C. Wang and P. F. Li, *Chem. - Eur. J.*, DOI: 10.1002/chem.202004477.
58. U. Novak and P. Žnidaršič-Plazl, *Green Process. Synth.*, 2013, **2**, 561-568.
59. U. Novak and P. Žnidaršič-Plazl, *J.Flow.Chem.*, 2016, **6**, 33-38.
60. A. Romanov, Z. Slouka and M. Přibyl, *Biotechnol. Bioeng.*, 2021, **118**, 715-724.
61. A. Pohar, P. Žnidaršič-Plazl and I. Plazl, *Chem. Eng. J.*, 2012, **189-190**, 376-382.
62. L. Vobecká, A. Romanov, Z. Slouka, P. Hasal and M. Přibyl, *New Biotechnol.*, 2018, **47**, 73-79.
63. F. A. Vicente, I. Plazl, S. P. M. Ventura and P. Žnidaršič-Plazl, *Green Chem.*, 2020, **22**, 4391-4410.
64. R. R. G. Soares, P. Novo, A. M. Azevedo, P. Fernandes, M. R. Aires-Barros, V. Chu and J. P. Conde, *Lab Chip*, 2014, **14**, 4284-4294.
65. A. Adamo, R. L. Beingessner, M. Behnam, J. Chen, T. F. Jamison, K. F. Jensen, J.-C. M. Monbaliu, A. S. Myerson, E. M. Revalor, D. R. Snead, T. Stelzer, N. Weeranoppanant, S. Y. Wong and P. Zhang, *Science*, 2016, **352**, 61.
66. T. Noël, S. Kuhn, A. J. Musacchio, K. F. Jensen and S. L. Buchwald, *Angew. Chem., Int. Ed.*, 2011, **50**, 5943-5946.
67. M. M. E. Delville, K. Koch, J. C. M. van Hest and F. Rutjes, *Org. Biomol. Chem.*, 2015, **13**, 1634-1638.
68. I. V. Gursel, F. Aldiansyah, Q. Wang, T. Noël and V. Hessel, *Chem. Eng. J.*, 2015, **270**, 468-475.
69. A. Adamo, R. L. Beingessner, M. Behnam, J. Chen, T. F. Jamison, K. F. Jensen, J.-C. M. Monbaliu, A. S. Myerson, E. M. Revalor, D. R. Snead, T. Stelzer, N. Weeranoppanant, S. Y. Wong and P. Zhang, *Science*, 2016, **352**, 61-67.
70. R. Lebl, T. Murray, A. Adamo, D. Cantillo and C. O. Kappe, *ACS Sustainable Chem. Eng.*, 2019, **7**, 20088-20096.
71. P. Desir, T.-Y. Chen, M. Bracconi, B. Saha, M. Maestri and D. G. Vlachos, *React. Chem. Eng.*, 2020, **5**, 39-50.
72. S. Caratzoulas, M. E. Davis, R. J. Gorte, R. Gounder, R. F. Lobo, V. Nikolakis, S. I. Sandler, M. A. Snyder, M. Tsapatsis and D. G. Vlachos, *J. Phys. Chem. C*, 2014, **118**, 22815-22833.
73. T. D. Swift, C. Bagia, V. Choudhary, G. Peklaris, V. Nikolakis and D. G. Vlachos, *ACS Catal.*, 2014, **4**, 259-267.
74. R. L. Barton, *Chem.Eng.*, 1974, **81**, 111-111.
75. M. E. Leblebici, S. Kuhn, G. D. Stefanidis and T. Van Gerven, *Chem. Eng. J.*, 2016, **293**, 273-280.
76. N. Weeranoppanant, A. Adamo, G. Saparbaiuly, E. Rose, C. Fleury, B. Schenkel and K. F. Jensen, *Ind. Eng. Chem. Res.*, 2017, **56**, 4095-4103.
77. Y. Shen, N. Weeranoppanant, L. Xie, Y. Chen, M. R. Lusardi, J. Imbrogno, M. G. Bawendi and K. F. Jensen, *Nanoscale*, 2017, **9**, 7703-7707.